Facial Landmark Detection
by Deep Multi-task Learning

Zhanpeng Zhang, Ping Luo, Chen Change Loy, and Xiaoou Tang

Dept. of Information Engineering, The Chinese University of Hong Kong,
Hong Kong, China

Abstract. Facial landmark detection has long been impeded by the problems of occlusion and pose variation. Instead of treating the detection task as a single and independent problem, we investigate the possibility of improving detection robustness through multi-task learning. Specifically, we wish to optimize facial landmark detection together with heterogeneous but subtly correlated tasks, e.g. head pose estimation and facial attribute inference. This is non-trivial since different tasks have different learning difficulties and convergence rates. To address this problem, we formulate a novel tasks-constrained deep model, with task-wise early stopping to facilitate learning convergence. Extensive evaluations show that the proposed task-constrained learning (i) outperforms existing methods, especially in dealing with faces with severe occlusion and pose variation, and (ii) reduces model complexity drastically compared to the state-of-the-art method based on cascaded deep model [21].

1 Introduction

Facial landmark detection is a fundamental component in many face analysis tasks, such as facial attribute inference [17], face verification [15, 22, 23, 35], and face recognition [33, 34]. Though great strides have been made in this field [8, 9, 10, 16], robust facial landmark detection remains a formidable challenge in the presence of partial occlusion and large head pose variations (Figure 1).

Facial landmark detection is traditionally approached as a single and independent problem. Popular approaches include template fitting approaches [8, 32, 27] and regression-based methods [3, 4, 9, 26, 31]. For example, Sun et al. [21] propose to detect facial landmarks by coarse-to-fine regression using a cascade of deep convolutional neural networks (CNN). This method shows superior accuracy compared to previous methods [2, 4] and existing commercial systems. Nevertheless, the method requires a complex and unwieldy cascade architecture of deep model.

We believe that facial landmark detection is not a standalone problem, but its estimation can be influenced by a number of heterogeneous and subtly correlated factors. For instance, when a kid is smiling, his mouth is widely opened (second image in Figure 1). Effectively discovering and exploiting such an intrinsically correlated facial attribute would help in detecting the mouth corners more accurately. Also, the inter-ocular distance is smaller in faces with large yaw
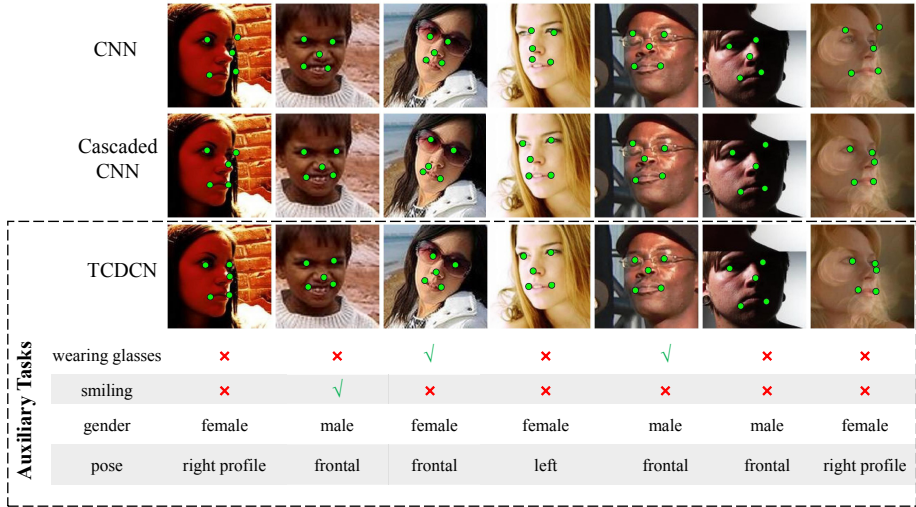
Auxiliary Tasks							
wearing glasses	✗	✗	√	✗	√	✗	✗
smiling	✗	√	✗	✗	✗	✗	✗
gender	female	male	female	female	male	male	female
pose	right profile	frontal	frontal	left	frontal	frontal	right profile

Fig. 1. Examples of facial landmark detection by a single conventional CNN, the cascaded CNN [21], and the proposed Tasks-Constrained Deep Convolutional Network (TCDCN). More accurate detection can be achieved by optimizing the detection task jointly with related/auxiliary tasks.

rotation (the last image in Figure 1). Such pose information can be leveraged as additional source of information to constrain the solution space of landmark estimation. Given the rich set of plausible related tasks, treating facial landmark detection in isolation is counterproductive.

This study aims to investigate the possibility of *optimizing facial landmark detection (the main task) with related/auxiliary tasks*, which include head pose estimation, gender classification, age estimation [6], facial expression recognition, or facial attribute inference [17]. There are several unique challenges. First, despite all the tasks share facial images as their common input, their output spaces and decision boundaries are different. Importantly, different tasks are inherently different in learning difficulties. For instance, learning to identify 'wearing glasses' attribute is easier than determining if one is smiling. In addition, we rarely have related task with similar number of positive/negative cases. Hence, different tasks have different convergence rates. Certain tasks are likely to be over-fitting earlier than the others when learning simultaneously, which could jeopardises the learning convergence of the whole model.

To this end, we propose a *Tasks-Constrained Deep Convolutional Network* (TCDCN) to jointly optimize facial landmark detection with a set of related tasks. Specifically, we formulate a task-constrained loss function to allow the errors of related tasks to be back-propagated jointly to improve the generalization of landmark detection. To accommodate related tasks with different learning difficulties and convergence rates, we devise a task-wise early stopping criterion to facilitate learning convergence. To show the usefulness of the proposed model, we select a diverse set of related tasks deliberately, as depicted in Figure 1. These

tasks include appearance attribute ('wearing glasses'), expression ('smiling'), demographic ('gender'), and head pose. Note that the proposed model does not limit the number of related tasks.

Contribution: Multi-task learning is not new (see Section 2), but to our knowledge, this is the first attempt to investigate how facial landmark detection can be optimized together with heterogeneous but subtly correlated tasks. We systematically show that multiple tasks share and learn common deep layers, so the representations learned from related tasks facilitate the learning of the main task. We further show that tasks relatedness are captured implicitly by the proposed model. The proposed approach outperforms the cascaded CNN model [21] and other existing methods [3, 4, 25, 27, 32]. Finally, we demonstrate the effectiveness of using our five-landmark estimation as robust initialization for improving a state-of-the-art face alignment method [3].

2   Related Work

Facial Landmark Detection: Conventional facial landmark detection methods can be divided into two categories, namely regression-based method and template fitting method. A regression-based method estimates landmark locations explicitly by regression using image features. For example, Valstar et al. [24] predict landmark location from local image patch with support vector regression. Cao et al. [4] and Burgos-Artizzu et al. [3] employ cascaded fern regression with pixel-difference features. A number of studies [9, 10, 26] use random regression forest to cast votes for landmark location based on local image patch with Haar-like features. Most of these methods refine an initial guess of the landmark location iteratively, the first guess/initialization is thus critical. By contrast, our deep model takes raw pixels as input without the need of any facial landmark initialization. Importantly, our method differs in that we exploit related tasks to facilitate landmark detection learning.

A template fitting method builds face templates to fit input images [8, 14]. Part-based model has recently been used for face fitting [1, 27, 32]. Zhu and Ramanan [32] show that face detection, facial landmark detection, and pose estimation can be jointly addressed. Our method differs in that we do not limit the learning of specific tasks, i.e. the TCDCN is readily expandable to be trained with additional related tasks. Specifically, apart from pose, we show that facial attribute, gender, and expression, can be useful for learning a robust landmark detector. Another difference to [32] is that we learn feature representation from raw pixels rather than pre-defined HOG as face descriptor.

Landmark Detection by CNN: The closest method to our approach is the cascaded CNN by Sun et al. [21]. The cascaded CNN requires a pre-partition of faces into different parts, each of which are processed by separate deep CNNs. The resulting outputs are subsequently averaged and channeled to separate cascaded layers to process each facial landmark individually. Our model requires neither pre-partition of faces nor cascaded layers, leading to drastic reduction in model complexity, whilst still achieving comparable or even better accuracy.

Multi-task Learning: The proposed approach falls under the big umbrella of multi-task learning. Multi-task learning has proven effective in many computer vision problems [28, 29]. Deep model is well suited for multi-task learning since the features learned from a task may be useful for other task. Existing multi-task deep models [7] are not suitable to solve our problem because they assume similar learning difficulties and convergence rates across all tasks. Specifically, the iterative learning on all tasks are performed without early stopping. Applying this assumption on our problem leads to difficulty in learning convergence, as shown in Section 4. We mitigate this shortcoming through task-wise early stopping. Early stopping is not uncommon in vision learning problems [13, 19]. Neural network methods [20] have also extensively used it to prevent over-fitting by halting the training process of a single task before a minimum error is achieved on the training set. Our early stopping scheme is inspired by Caruana [5], but his study is limited to shallow multilayer perceptrons. We show that early stopping is equally important for multi-task deep convolutional network.

3   Tasks-Constrained Facial Landmark Detection

3.1   Problem Formulation

The traditional multi-task learning (MTL) seeks to improve the generalization performance of multiple related tasks by learning them jointly. Suppose we have a total of T tasks and the training data for the t-th task are denoted as $(\mathbf{x}_i^t, y_i^t)$, where $t = \{1, \ldots, T\}$, $i = \{1, \ldots, N\}$, with $\mathbf{x}_i^t \in \mathbb{R}^d$ and $y_i^t \in \mathbb{R}$ being the feature vector and label, respectively[1]. The goal of the MTL is to minimize

$$\underset{\{\mathbf{w}^t\}_{t=1}^T}{\operatorname{argmin}} \sum_{t=1}^{T} \sum_{i=1}^{N} \ell(y_i^t, f(\mathbf{x}_i^t; \mathbf{w}^t)) + \Phi(\mathbf{w}^t), \tag{1}$$

where $f(\mathbf{x}^t; \mathbf{w}^t)$ is a function of $\mathbf{x}^t$ and parameterized by a weight vector $\mathbf{w}^t$. The loss function is denoted by $\ell(\cdot)$. A typical choice is the least square for regression and the hinge loss for classification. The $\Phi(\mathbf{w}^t)$ is the regularization term that penalizes the complexity of weights.

In contrast to conventional MTL that maximizes the performance of all tasks, our aim is to optimize the main task r, which is facial landmark detection, with the assistances of arbitrary number of related/auxiliary tasks $a \in A$. Examples or related tasks include facial pose estimation and attribute inference. To this end, our problem can be formulated as

$$\underset{\mathbf{W}^r, \{\mathbf{W}^a\}_{a \in A}}{\operatorname{argmin}} \sum_{i=1}^{N} \ell^r(y_i^r, f(\mathbf{x}_i; \mathbf{W}^r)) + \sum_{i=1}^{N} \sum_{a \in A} \lambda^a \ell^a(y_i^a, f(\mathbf{x}_i; \mathbf{W}^a)), \tag{2}$$

---

[1] In this paper, scalar, vector, and matrix are denoted by lowercase, bold lowercase, and bold capital letter, respectively.

where λ^a denotes the importance coefficient of a-th task's error and the regularization terms are omitted for simplification. Beside the aforementioned difference, Eq.(1) and Eq.(2) are distinct in two aspects. First, different types of loss functions can be optimized together by Eq.(2), e.g. regression and classification can be combined, while existing methods [30] that employ Eq.(1) assume implicitly that the loss functions across all tasks are identical. Second, Eq.(1) allows data $\mathbf{x}_i^t$ in different tasks to have different input representations, while Eq.(2) focuses on a shared input representation $\mathbf{x}_i$. The latter is more suitable for our problem, since all tasks share similar facial representation.

In the following, we formulate our facial landmark detection model based on Eq.(2). Suppose we have a set of feature vectors in a shared feature space across tasks $\{\mathbf{x}_i\}_{i=1}^N$ and their corresponding labels $\{\mathbf{y}_i^r, y_i^p, y_i^g, y_i^w, y_i^s\}_{i=1}^N$, where $\mathbf{y}_i^r$ is the target of landmark detection and the remaining are the targets of auxiliary tasks, including inferences of 'pose', 'gender', 'wear glasses', and 'smiling'. More specifically, $\mathbf{y}_i^r \in \mathbb{R}^{10}$ is the 2D coordinates of the five landmarks (centers of the eyes, nose, corners of the mouth), $y_i^p \in \{0, 1, .., 4\}$ indicates five different poses $(0°, \pm30°, \pm60°)$, and $y_i^g, y_i^w, y_i^s \in \{0, 1\}$ are binary attributes. It is reasonable to employ the least square and cross-entropy as the loss functions for the main task (regression) and the auxiliary tasks (classification), respectively. Therefore, the objective function can be rewritten as

$$\operatorname*{argmin}_{\mathbf{W}^r, \{\mathbf{W}^a\}} \frac{1}{2} \sum_{i=1}^N \|\mathbf{y}_i^r - f(\mathbf{x}_i; \mathbf{W}^r)\|^2 - \sum_{i=1}^N \sum_{a \in A} \lambda^a y_i^a \log(p(y_i^a | \mathbf{x}_i; \mathbf{W}^a)) + \sum_{t=1}^T \|\mathbf{W}\|_2^2, \tag{3}$$

where $f(\mathbf{x}_i; \mathbf{W}^r) = (\mathbf{W}^r)^\mathsf{T} \mathbf{x}_i$ in the first term is a linear function. The second term is a softmax function $p(y_i = m | \mathbf{x}_i) = \frac{\exp\{(\mathbf{W}_m^a)^\mathsf{T} \mathbf{x}_i\}}{\sum_j \exp\{(\mathbf{W}_j^a)^\mathsf{T} \mathbf{x}_i\}}$, which models the class posterior probability ($\mathbf{W}_j^a$ denotes the jth column of the matrix), and the third term penalizes large weights ($W = \{\mathbf{W}^r, \{\mathbf{W}^a\}\}$). In this work, we adopt the deep convolutional network (DCN) to jointly learn the share feature space $\mathbf{x}$, since the unique structure of DCN allows for multitask and shared representation.

In particular, given a face image $\mathbf{x}^0$, the DCN projects it to higher level representation gradually by learning a sequence of non-linear mappings

$$\mathbf{x}^0 \xrightarrow{\sigma\left((\mathbf{W}^{s_1})^\mathsf{T} \mathbf{x}^0\right)} \mathbf{x}^1 \xrightarrow{\sigma\left((\mathbf{W}^{s_2})^\mathsf{T} \mathbf{x}^1\right)} ... \xrightarrow{\sigma\left((\mathbf{W}^{s_l})^\mathsf{T} \mathbf{x}^{l-1}\right)} \mathbf{x}^l. \tag{4}$$

Here, $\sigma(\cdot)$ and $\mathbf{W}^{s_l}$ indicate the non-linear activation function and the filters needed to be learned in the layer l of DCN. For instance, $\mathbf{x}^l = \sigma\left((\mathbf{W}^{s_l})^\mathsf{T} \mathbf{x}^{l-1}\right)$. Note that $\mathbf{x}^l$ is the shared representation between the main task r, and related tasks A. Eq.(4) and Eq.(3) can be trained jointly. The former learns the shared space and the latter optimizes the tasks with respect to this space, and then the errors of the tasks can be propagated back to refine the space. We iterate this learning procedure until convergence. We call the learned model as Tasks-Constrained Deep Convolutional Network (TCDCN).
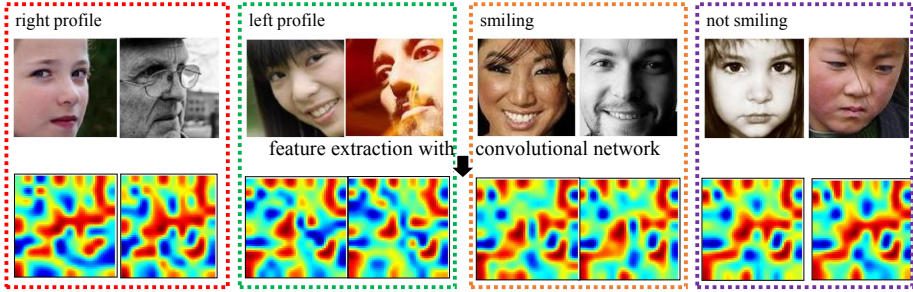
Fig. 2. The TCDCN extracts shared features for facial landmark detection and related tasks. The first row shows the face images and the second row shows the corresponding features in the shared feature space, where the face images with similar poses and attributes are close with each other. This reveals that the learned feature space is robust to pose, expression ('smiling'), and occlusion ('wearing glasses').

The TCDCN has four convolutional layers and a fully connected layer on the top. Each convolutional layer is followed by a max pooling layer. It is worth noting that in comparison to the cascaded CNN approach [21] that deploys 23 CNNs, our formulation constructs only one single CNN, of which complexity is similar to that of a CNN in the first-level cascade of [21]. We compare the complexity of these two approaches in Section 4.3. Further details of the network architecture is provided in Section 4 to facilitate re-implementation of the proposed model. Several pairs of face images and their features of the shared space of TCDCN are visualized in Figure 2, which shows that the learned features are robust to large poses and expressions. For example, the features of smiling faces or faces have similar poses exhibit similar patterns.

3.2   Learning Tasks-Constrained Deep Convolutional Network

A straightforward way to learn the proposed network is by stochastic gradient descent, whose effectiveness has been proven when a single task is present [12]. However, it is non-trivial to optimize multiple tasks simultaneously using the same method. The reason is that different tasks have different loss functions and learning difficulties, and thus with different convergence rates. Existing methods [30] solve this problem by exploring the relationship of tasks, e.g. through learning a covariance matrix of the weights of all tasks. Nevertheless, such methods can only be applied if the loss functions of all tasks are identical. This assumption is not valid when we wish to perform joint learning on heterogeneous tasks. Moreover, it is computationally impractical in dealing with weight vectors in high dimension.

Task-Wise Early Stopping: We propose an efficient yet effective approach to "early stop" the auxiliary tasks, before they begin to over-fit the training set and thus harm the main task. The intuition behind is that at the beginning

of the training process, the TCDCN is constrained by all tasks to avoid being trapped at a bad local minima. As training proceeds, certain auxiliary tasks are no longer beneficial to the main task after they reach their peak performance, their learning process thus should be halted. Note that the regularization offered by early stopping is different from weight regularization in Eq.(3). The latter globally helps to prevent over-fitting in each task through penalizing certain parameter configurations. In Section 4.2, we show that task-wise early stopping is critical for multi-task learning convergence even with weight regularization.

Now we introduce a criterion to automatically determine when to stop learning an auxiliary task. Let E_{val}^a and E_{tr}^a be the values of the loss function of task a on the validation set and training set, respectively. We stop the task if its measure exceeds a threshold ϵ as below

$$\frac{k \cdot \mathrm{med}_{j=t-k}^{t} E_{tr}^a(j)}{\sum_{j=t-k}^{t} E_{tr}^a(j) - k \cdot \mathrm{med}_{j=t-k}^{t} E_{tr}^a(j)} \cdot \frac{E_{val}^a(t) - \min_{j=1..t} E_{tr}^a(j)}{\lambda^a \cdot \min_{j=1..t} E_{tr}^a(j)} > \epsilon, \quad (5)$$

where t denotes the current iteration and k controls a training strip of length k. The 'med' denotes the function for calculating median value. The first term in Eq.(5) represents the tendency of the training error. If the training error drops rapidly within a period of length k, the value of the first term is small, indicating that training can be continued as the task is still valuable; otherwise, the first term is large, then the task is more likely to be stopped. The second term measures the generalization error compared to the training error. The λ^a is the importance coefficient of a-th task's error, which can be learned through gradient descent. Its magnitude reveals that more important task tends to have longer impact. This strategy achieves satisfactory results for learning deep convolution network given multiple tasks. Its superior performance is demonstrated in Section 4.2.

Learning Procedure: We have discussed when and how to switch off an auxiliary task during training before it over-fits. For each iteration, we perform stochastic gradient descent to update the weights of the tasks and filters of the network. For example, the weight matrix of the main task is updated by $\Delta \mathbf{W}^r = -\eta \frac{\partial E^r}{\partial \mathbf{W}^r}$ with η being the learning rate ($\eta = 0.003$ in our implementation), and $\frac{\partial E^r}{\partial \mathbf{W}^r} = (\mathbf{y}_i^r - (\mathbf{W}^r)^\mathsf{T} \mathbf{x}_i) \mathbf{x}_i^\mathsf{T}$. Also, the derivative of the auxiliary task's weights can be calculated in a similar manner as $\frac{\partial E^a}{\partial \mathbf{W}^a} = (p(y_i^a | \mathbf{x}_i; \mathbf{W}^a) - y_i^a) \mathbf{x}_i$. For the filters in the lower layer, we compute the gradients by propagating the loss error back following the back-propagation strategy as

$$\varepsilon^1 \xleftarrow{(\mathbf{W}^{s2})^\mathsf{T} \varepsilon^2 \frac{\partial \sigma(u^1)}{\partial u^1}} \varepsilon^2 \xleftarrow{(\mathbf{W}^{s3})^\mathsf{T} \varepsilon^3 \frac{\partial \sigma(u^2)}{\partial u^2}} ... \xleftarrow{(\mathbf{W}^{sl})^\mathsf{T} \varepsilon^l \frac{\partial \sigma(u^{l-1})}{\partial u^{l-1}}} \varepsilon^l, \quad (6)$$

where ε^l is the error at the shared representation layer and $\varepsilon^l = (\mathbf{W}^r)^\mathsf{T} [\mathbf{y}_i^r - (\mathbf{W}^r)^\mathsf{T} \mathbf{x}_i] + \sum_{a \in A} (p(y_i^a | \mathbf{x}_i; \mathbf{W}^a) - y_i^a) \mathbf{W}^a$, which is the integration of all tasks' derivatives. The errors of the lower layers are computed following Eq.(6). For instance, $\varepsilon^{l-1} = (\mathbf{W}^{sl})^\mathsf{T} \varepsilon^l \frac{\partial \sigma(u^{l-1})}{\partial u^{l-1}}$, where $\frac{\partial \sigma(u)}{\partial u}$ is the gradient of the activation function. Then, the gradient of the filter is obtained by $\frac{\partial E}{\partial \mathbf{W}^{sl}} = \varepsilon^l \mathbf{x}_\Omega^{l-1}$, where Ω represents the receptive field of the filter.

Prediction: First, a test face image $\mathbf{x}^0$ is projected to the shared space to obtain $\mathbf{x}^l$. Second, we predict the landmark positions by $(\mathbf{W}^r)^\mathsf{T}\mathbf{x}^l$ and the results of the auxiliary tasks by $p(y^a|\mathbf{x}^l; \mathbf{W}^a)$. This process is efficient and its complexity is discussed in Section 4.3.

4   Implementation and Experiments

Network Structure: Figure 3 shows the network structure of TCDCN. The input of the network is 40×40 gray-scale face image. The feature extraction stage contains four convolutional layers, three pooling layers, and one fully connected layer. Each convolutional layer contains a filter bank producing multiple feature maps. The filter weights are not spatially shared, that means a different set of filters is applied at every location in the input map. The absolute tangent function is selected as the activation function. For the pooling layers, we conduct max-pooling on non-overlap regions of the feature map. The fully connected layer following the fourth convolutional layer produces a feature vector which is shared by the multiple tasks in the estimation stage.
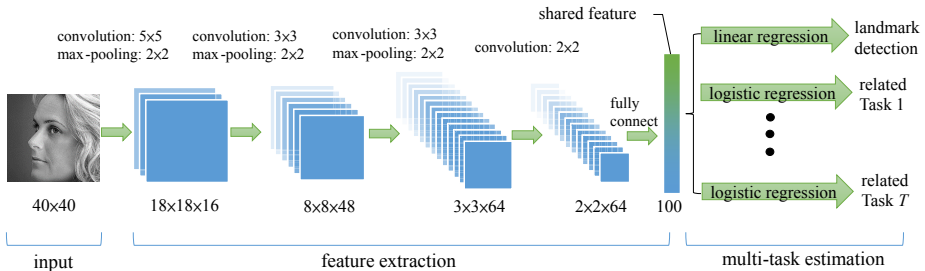
Fig. 3. Structure specification for TCDCN

Model Training: The training dataset we use is identical to [21], consisting of 10,000 outdoor face images from the web. Each image is annotated with bounding box and five landmarks, i.e. centers of the eyes, nose, corners of the mouth, as depicted in Figure 1. We augmented the training samples by small jittering, including translation, in-plane rotation, and zooming. The ground truths of the related tasks are labeled manually. This dataset, known as Multi-Task Facial Landmark (MTFL) dataset, and the landmark detector will be released for research usage[2].

Evaluation Metrics: In all cases, we report our results on two popular metrics [3, 4, 10, 21], including mean error and failure rate. The mean error is measured by the distances between estimated landmarks and the ground truths, normalizing with respect to the inter-ocular distance. Mean error larger than 10% is reported as a failure.
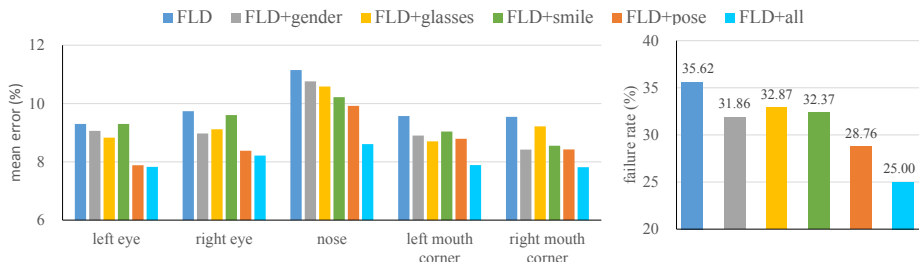
---

[2] http://mmlab.ie.cuhk.edu.hk/projects/TCDCN.html

Fig. 4. Comparison of different model variants of TCDCN: the mean error over different landmarks, and the overall failure rate

4.1 Evaluating the Effectiveness of Learning with Related Task

To examine the influence of related tasks, we evaluate five variants of the proposed model. In particular, the first variant is trained only on facial landmark detection. We train another four model variants on facial landmark detection along with the auxiliary task of recognizing 'pose', 'gender', 'wearing glasses', and 'smiling', respectively. The full model is trained using all the four related tasks. For simplicity, we name each variants by facial landmark detection (FLD) and the related task, such as "FLD", "FLD+pose", "FLD+all". We employ the popular AFLW [11] for evaluation. This dataset is selected because it is more challenging than other datasets, such as LFPW [2]. For example, AFLW has larger pose variations (39% of faces are non-frontal in our testing images) and severe partial occlusions. Figure 10 provides some examples. We selected 3,000 faces randomly from AFLW for testing.

It is evident from Figure 4 that optimizing landmark detection with related tasks are beneficial. In particular, FLD+all outperforms FLD by a large margin, with a reduction over 10% in failure rate. When single related task is present, FLD+pose performs the best. This is not surprising since pose variation affects locations of all landmarks globally and directly. The other related tasks such as 'smiling' and 'wearing glasses' are observed to have comparatively smaller influence to the final performance, since they mainly capture local information of the face, such as mouth and eyes. We examine two specific cases below.

FLD vs. FLD+smile: As shown in Figure 5, landmark detection benefits from smiling attribute inference, mainly at the nose and corners of mouth. This observation is intuitive since smiling drives the lower part of the faces, involving Zygomaticus and levator labii superioris muscles, more than the upper facial region. The learning of smile attributes develops a shared representation that describes lower facial region, which in turn facilitates the localization of nose and corners of mouth.

We use a crude method to investigate the relationship between tasks. Specifically, we study the Pearson's correlation of the learned weight vectors of the last fully-connected layer, between the tasks of facial landmark detection and 'smiling' prediction, as shown in Figure 5(b). The correlational relationship is indicative to the performance improvement depicted in Figure 5(a). For instance, the
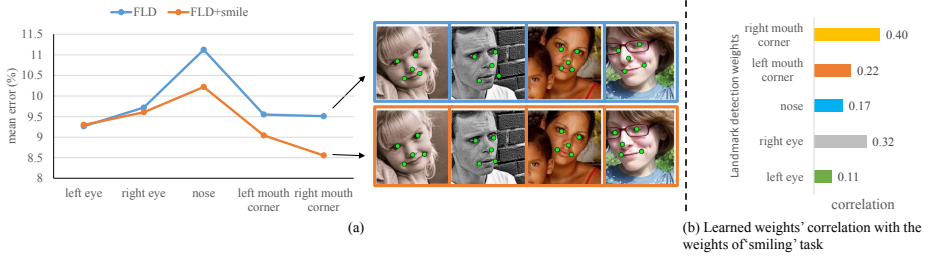
(a)

(b) Learned weights' correlation with the weights of 'smile' task

Fig. 5. FLD vs. FLD+smile. The smiling attribute helps detection more on the nose and corners of mouth, than the centers of eyes, since 'smiling' mainly affects the lower part of a face.
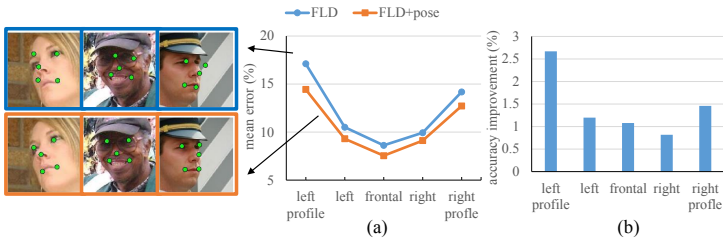

Fig. 6. FLD vs. FLD+pose. (a) Mean error in different poses, and (b) Accuracy improvement by the FLD+pose in different poses.

weight vectors, which are learned to predict the positions of the mouth's corners have high correlation with the weights of 'smiling' inference. This demonstrates that TCDCN implicitly learns relationship between tasks.

FLD vs. FLD+pose: As observed in Figure 6(a), detection errors of FLD increase along with the degree of head pose deviation from the frontal view to profiles, while these errors can be partially recovered by FLD+pose as depicted in Figure 6(b).

4.2   The Benefits of Task-Wise Early Stopping

To verify the effectiveness of the task-wise early stopping, we train the proposed TCDCN with and without this technique and compare the landmark detection rates in Figure 7(a), which shows that without task-wise early stopping, the accuracy is much lower. Figure 7(b) plots the main task's loss errors of the training set and the validation set within 2,600 iterations. Without early stopping, the training error converges slowly and exhibits substantial oscillations. However, convergence rates of both the training and validation sets are fast and stable when using the proposed early stopping scheme. In Figure 7(b), we also point out when and which task has been halted during the training procedure. For example, 'wearing glasses' and 'gender' are stopped at the 250th and 350th iterations, and 'pose' lasts to the 750th iteration, which matches our expectation that 'pose' has the largest benefit to landmark detection, compared to the other related tasks.
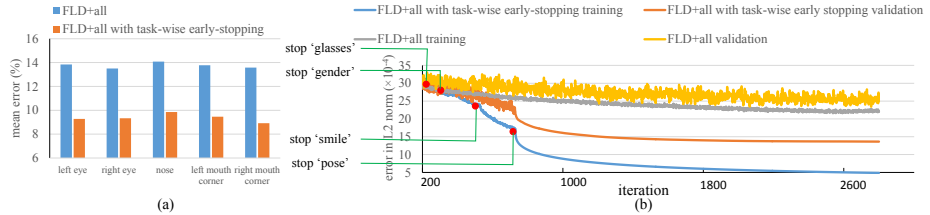
Fig. 7. (a) Task-wise early stopping leads to substantially lower validation errors over different landmarks. (b) Its benefit is also reflected on the training and validation error convergence rate. The error is measured in L2-norm with respect to the ground truth of the 10 coordinates values (normalized to [0,1]) for the 5 landmarks.

4.3   Comparison with the Cascaded CNN [21]

Although both the TCDCN and the cascaded CNN [21] are built upon CNN, we show that the proposed model can achieve better detection accuracy with a significantly lower computational cost. We use the full model "FLD+all", and the publicly available binary code of the cascaded CNN in this experiment.

Landmark Localization Accuracy: Similar to Section 4.1, we employ AFLW images for evaluation due to its challenging pose variations and occlusion. Note that we use the same 10,000 training faces as in the cascaded CNN method. Thus the only difference is that we exploit a multi-task learning approach. It is observed from Figure 8 that our method performs better in four out of five landmarks, and the overall accuracy is superior to that of cascaded CNN.
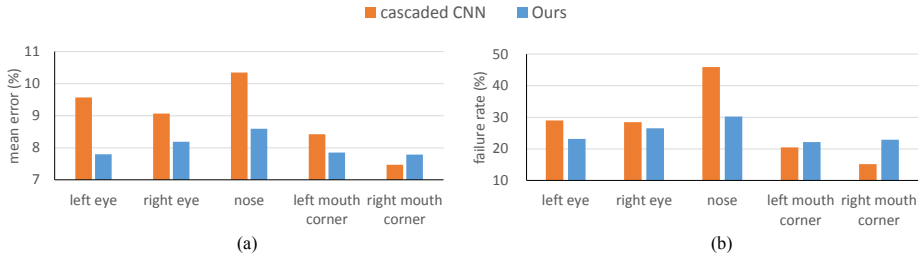

Fig. 8. The proposed TCDCN vs. cascaded CNN [21]: (a) mean error over different landmarks and (b) the overall failure rate

Computational Efficiency: Suppose the computation time of a 2D-convolution operation is τ, the total time cost for a CNN with L layers can be approximated by $\sum_{l=1}^{L} s_l^2 q_l q_{l-1} \tau$, where s^2 is the 2D size of the input feature map for l-th layer, and q is the number of filters. The algorithm complexity of a CNN is thus $O(s^2 q^2)$, directly related to the input image size and number of filters. Note that the input face size and network structure for TCDCN is similar to cascaded CNN. The proposed method only has one CNN, whereas the cascaded CNN [21] deploys multiple CNNs in different cascaded layers (23 CNNs in its implementation). Hence, TCDCN has much lower computational cost. The cascaded CNN
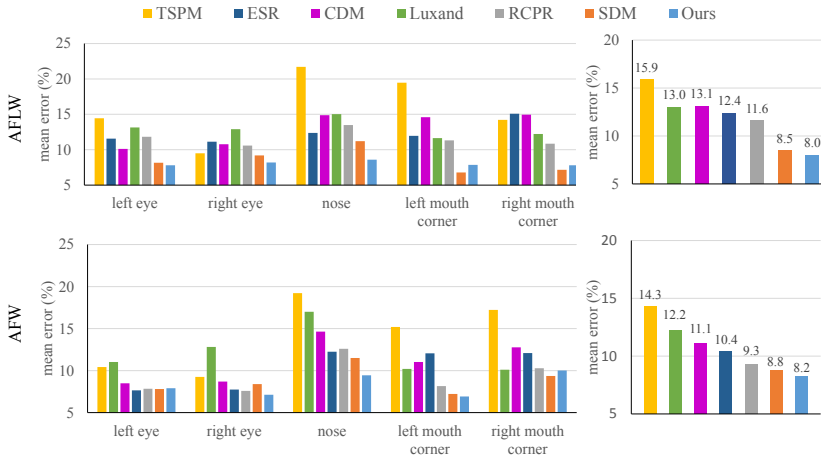
Fig. 9. Comparison with RCPR [3], TSPM [32], CDM [27], Luxand [18], and SDM [25] on AFLW [11] (the first row) and AFW [32] (the second row) datasets. The left subfigures show the mean errors on different landmarks, while the right subfigures show the overall errors.

requires 0.12s to process an image on an Intel Core i5 CPU, whilst TCDCN only takes 17ms, which is *7 times faster*. The TCDCN costs 1.5ms on a NVIDIA GTX760 GPU.

4.4   Comparison with Other State-of-the-Art Methods

We compare against: (1) Robust Cascaded Pose Regression (RCPR) [3] using the publicly available implementation and parameter settings; (2) Tree Structured Part Model (TSPM) [32], which jointly estimates the head pose and facial landmarks; (3) A commercial software, Luxand face SDK [18]; (4) Explicit Shape Regression (ESR) [4]; (5) A Cascaded Deformable Model (CDM) [27]; (6) Supervised Descent Method (SDM) [25]. For the methods which include their own face detector (TSPM [32] and CDM [27]), we avoid detection errors by cropping the image around the face.

Evaluation on AFLW [11]: Figure 9 shows that TCDCN outperforms all the state-of-the-art methods. Figure 10(a) shows several examples of TCDCN's detection, with additional tags generated from related tasks. We observe that the proposed method is robust to faces with large pose variation, lighting, and severe occlusion. It is worth pointing out that the input images of our model is 40×40, which means that the model can cope with low-resolution images.

Evaluation on AFW [32]: In addition to AFLW, we also tested on AFW. We observe similar trend as in the AFLW dataset. Figure 9 demonstrates the superiority of our method. Figure 10(b) presents some detection examples using our model.
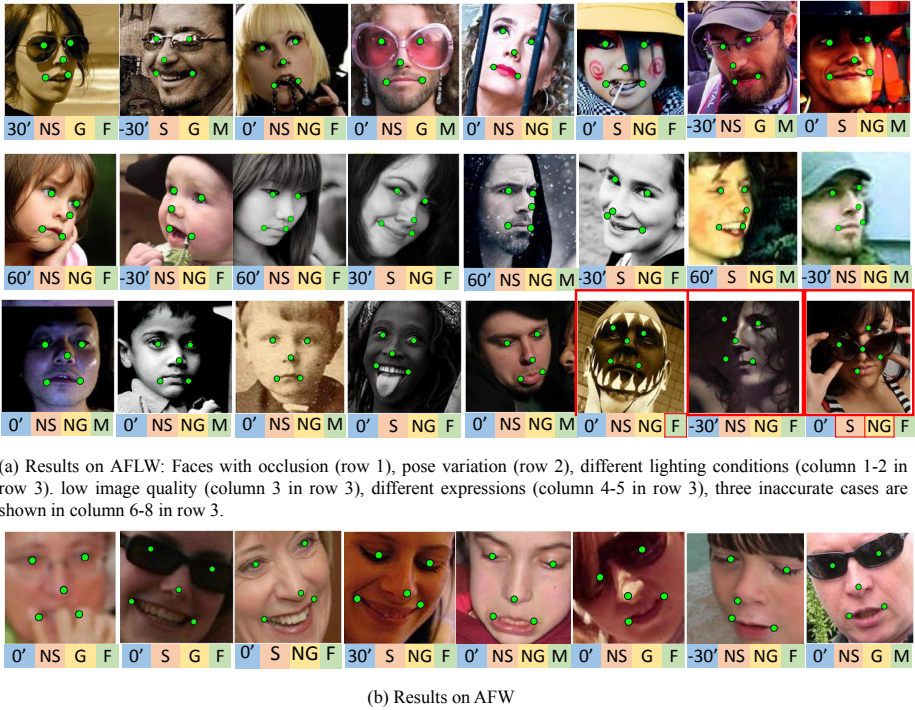
(a) Results on AFLW: Faces with occlusion (row 1), pose variation (row 2), different lighting conditions (column 1-2 in row 3). low image quality (column 3 in row 3), different expressions (column 4-5 in row 3), three inaccurate cases are shown in column 6-8 in row 3.

(b) Results on AFW

Fig. 10. Example detections by the proposed model on AFLW [11] and AFW [32] images. The labels below each image denote the tagging results for the related tasks: $(0°, ±30°, ±60°)$ for pose; S/NS = smiling/not-smiling; G/NG = with-glasses/without-glasses; M/F = male/female. Red rectangles indicate wrong tagging.
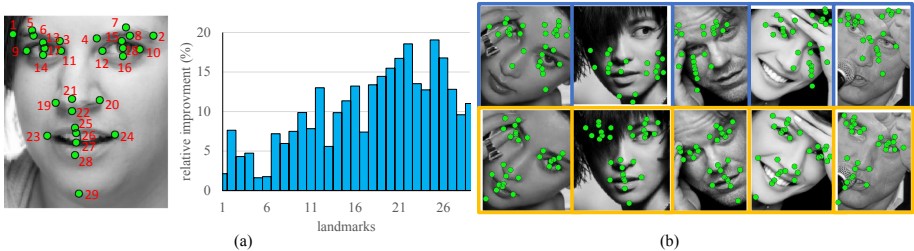

Fig. 11. Initialization with our five-landmark estimation for RCPR [3] on COFW dataset [3]. (a) shows the relative improvement on each landmark (relative improvement $= \frac{\text{reduced error}}{\text{original error}}$). (b) visualizes the improvement. The upper row depicts the results of RCPR [3], while the lower row shows the improved results by our initialization.

4.5 TCDCN for Robust Initialization

This section shows that the TCDCN can be used to generate a good initialization to improve the state-of-the-art method, owing to its accuracy and efficiency. We

take RCPR [3] as an example. Instead of drawing training samples randomly as initialization as did in [3], we initialize RCPR by first applying TCDCN on the test image to estimate the five landmarks. We compare the results of RCPR with and without TCDCN as initialization on the COFW dataset [3], which includes 507 test faces that are annotated with 29 landmarks. Figure 11(a) shows the relative improvement for each landmark on the COFW dataset and Figure 11(b) visualizes several examples. It is demonstrated that with our robust initialization, the algorithm can obtain improvement in difficult cases with rotation and occlusion.

5   Conclusions

Instead of learning facial landmark detection in isolation, we have shown that more robust landmark detection can be achieved through joint learning with heterogeneous but subtly correlated tasks, such as appearance attribute, expression, demographic, and head pose. The proposed Tasks-Constrained DCN allows errors of related tasks to be back-propagated in deep hidden layers for constructing a shared representation to be relevant to the main task. We have shown that task-wise early stopping scheme is critical to ensure convergence of the model. Thanks to multi-task learning, the proposed model is more robust to faces with severe occlusions and large pose variations compared to existing methods. We have observed that a deep model needs not be cascaded [21] to achieve the better performance. The lighter-weight CNN allows real-time performance without the usage of GPU or parallel computing techniques. Future work will explore deep multi-task learning for dense landmark detection and other vision domains.

References

1. Asthana, A., Zafeiriou, S., Cheng, S., Pantic, M.: Robust discriminative response map fitting with constrained local models. In: CVPR, pp. 3444–3451 (2013)
2. Belhumeur, P.N., Jacobs, D.W., Kriegman, D.J., Kumar, N.: Localizing parts of faces using a consensus of exemplars. In: CVPR, pp. 545–552 (2011)
3. Burgos-Artizzu, X.P., Perona, P., Dollar, P.: Robust face landmark estimation under occlusion. In: ICCV, pp. 1513–1520 (2013)
4. Cao, X., Wei, Y., Wen, F., Sun, J.: Face alignment by explicit shape regression. In: CVPR, pp. 2887–2894 (2012)
5. Caruana, R.: Multitask learning. Machine Learning 28(1), 41–75 (1997)
6. Chen, K., Gong, S., Xiang, T., Loy, C.C.: Cumulative attribute space for age and crowd density estimation. In: CVPR, pp. 2467–2474 (2013)
7. Collobert, R., Weston, J.: A unified architecture for natural language processing: Deep neural networks with multitask learning. In: ICML, pp. 160–167 (2008)
8. Cootes, T.F., Edwards, G.J., Taylor, C.J.: Active appearance models. PAMI 23(6), 681–685 (2001)
9. Cootes, T.F., Ionita, M.C., Lindner, C., Sauer, P.: Robust and accurate shape model fitting using random forest regression voting. In: Fitzgibbon, A., Lazebnik, S., Perona, P., Sato, Y., Schmid, C. (eds.) ECCV 2012, Part VII. LNCS, vol. 7578, pp. 278–291. Springer, Heidelberg (2012)

10. Dantone, M., Gall, J., Fanelli, G., Van Gool, L.: Real-time facial feature detection using conditional regression forests. In: CVPR, pp. 2578–2585 (2012)
11. Kostinger, M., Wohlhart, P., Roth, P.M., Bischof, H.: Annotated facial landmarks in the wild: A large-scale, real-world database for facial landmark localization. In: ICCV Workshops, pp. 2144–2151 (2011)
12. Krizhevsky, A., Sutskever, I., Hinton, G.E.: Imagenet classification with deep convolutional neural networks. In: NIPS (2012)
13. Li, H., Shen, C., Shi, Q.: Real-time visual tracking using compressive sensing. In: CVPR, pp. 1305–1312 (2011)
14. Liu, X.: Generic face alignment using boosted appearance model. In: CVPR (2007)
15. Lu, C., Tang, X.: Surpassing human-level face verification performance on LFW with GaussianFace. Tech. rep., arXiv:1404.3840 (2014)
16. Luo, P., Wang, X., Tang, X.: Hierarchical face parsing via deep learning. In: CVPR, pp. 2480–2487 (2012)
17. Luo, P., Wang, X., Tang, X.: A deep sum-product architecture for robust facial attributes analysis. In: CVPR, pp. 2864–2871 (2013)
18. Luxand Incorporated: Luxand face SDK, http://www.luxand.com/
19. Nair, V., Hinton, G.E.: Rectified linear units improve restricted boltzmann machines. In: ICML, pp. 807–814 (2010)
20. Prechelt, L.: Automatic early stopping using cross validation: quantifying the criteria. Neural Networks 11(4), 761–767 (1998)
21. Sun, Y., Wang, X., Tang, X.: Deep convolutional network cascade for facial point detection. In: CVPR, pp. 3476–3483 (2013)
22. Sun, Y., Wang, X., Tang, X.: Deep learning face representation by joint identification-verification. Tech. rep., arXiv:1406.4773 (2014)
23. Sun, Y., Wang, X., Tang, X.: Deep learning face representation from predicting 10,000 classes. In: CVPR (2014)
24. Valstar, M., Martinez, B., Binefa, X., Pantic, M.: Facial point detection using boosted regression and graph models. In: CVPR, pp. 2729–2736 (2010)
25. Xiong, X., De La Torre, F.: Supervised descent method and its applications to face alignment. In: CVPR, pp. 532–539 (2013)
26. Yang, H., Patras, I.: Sieving regression forest votes for facial feature detection in the wild. In: ICCV, pp. 1936–1943 (2013)
27. Yu, X., Huang, J., Zhang, S., Yan, W., Metaxas, D.N.: Pose-free facial landmark fitting via optimized part mixtures and cascaded deformable shape model. In: ICCV, pp. 1944–1951 (2013)
28. Yuan, X.T., Liu, X., Yan, S.: Visual classification with multitask joint sparse representation. TIP 21(10), 4349–4360 (2012)
29. Zhang, T., Ghanem, B., Liu, S., Ahuja, N.: Robust visual tracking via structured multi-task sparse learning. IJCV 101(2), 367–383 (2013)
30. Zhang, Y., Yeung, D.Y.: A convex formulation for learning task relationships in multi-task learning. In: UAI (2011)
31. Zhang, Z., Zhang, W., Liu, J., Tang, X.: Facial landmark localization based on hierarchical pose regression with cascaded random ferns. In: ACM Multimedia, pp. 561–564 (2013)
32. Zhu, X., Ramanan, D.: Face detection, pose estimation, and landmark localization in the wild. In: CVPR, pp. 2879–2886 (2012)
33. Zhu, Z., Luo, P., Wang, X., Tang, X.: Deep learning identity-preserving face space. In: ICCV, pp. 113–120 (2013)
34. Zhu, Z., Luo, P., Wang, X., Tang, X.: Deep learning multi-view representation for face recognition. Tech. rep., arXiv:1406.6947 (2014)
35. Zhu, Z., Luo, P., Wang, X., Tang, X.: Recover canonical-view faces in the wild with deep neural networks. Tech. rep., arXiv:1404.3543 (2014)